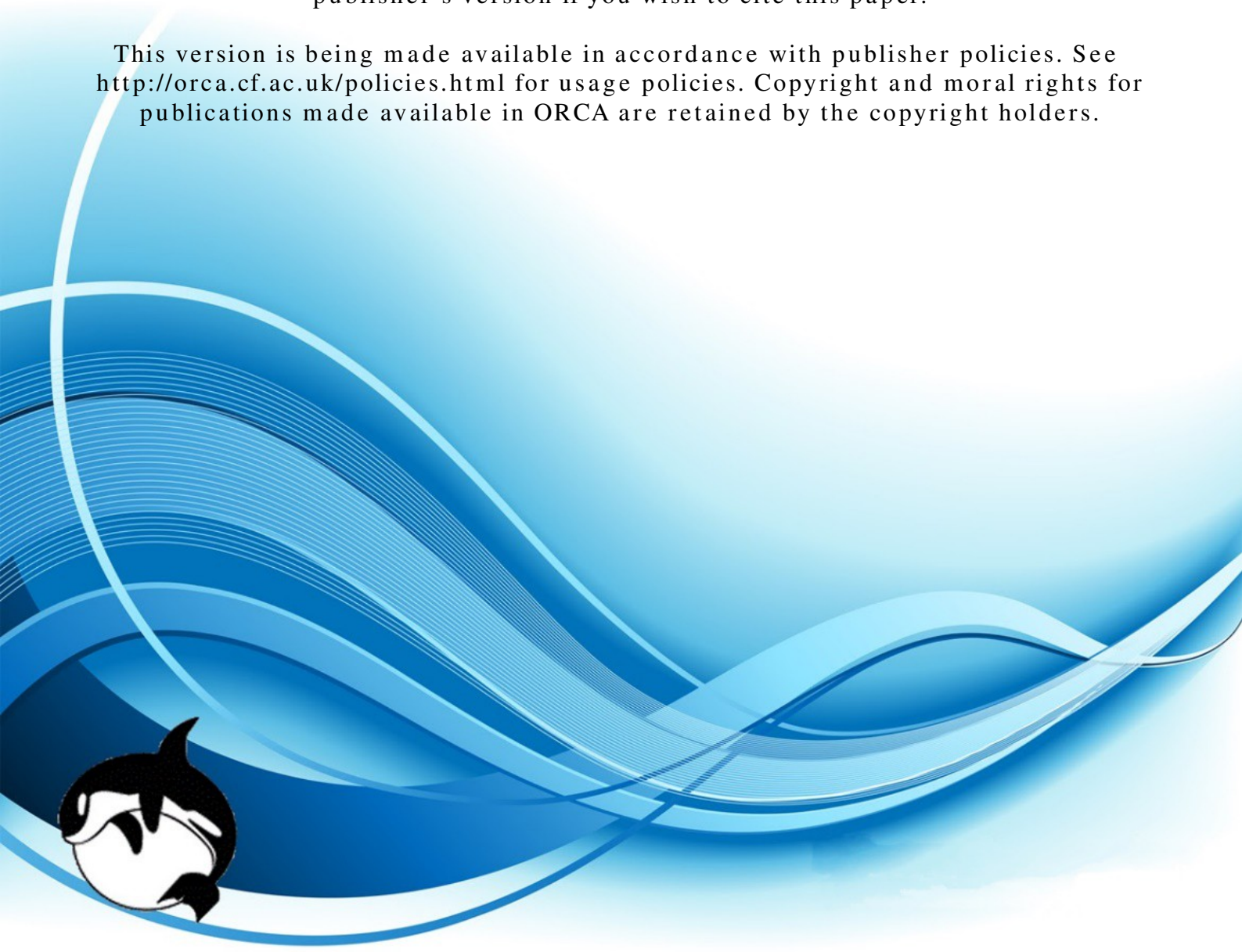

Environmental assessment of underground coal gasification in deep-buried seams

- Ni An, PhD, MSc, BSc; (Corresponding author: Ann@cardiff.ac.uk)
- Research Associate, Geoenvironmental Research Centre (GRC), Cardiff School of Engineering, Cardiff University, Cardiff, Wales, UK
- Department of Civil Engineering, Zhejiang University, Hangzhou 310058, China

- Renato Zagorščak, PhD, MSc, BSc;
- Research Associate, Geoenvironmental Research Centre (GRC), Cardiff School of Engineering, Cardiff University, Cardiff, Wales, UK

- Hywel Rhys Thomas, BSc, MSc, DIC, PhD, DSc, ACIPR, CEng, FGS, FREng, FRS, FLSW, MAE;
- Professor and Director, Geoenvironmental Research Centre (GRC), Cardiff School of Engineering, Cardiff University, Cardiff, Wales, UK

Abstract: This study presents a preliminary assessment of the environmental impact of field-scale underground coal gasification (UCG) targeting deep-buried seams by studying the fate of the UCG products in the reactor vicinity. A series of simulation scenarios are conducted in three deep (900 m) areas of specific interest, i.e. South Wales coalfield (UK), Upper Silesian coal Basin (PL), and Ruhr mining district (DE), to investigate the gaseous and dissolved chemicals' transport. The results indicate that the syngas propagation is limited to 2.0 m in the reactor's vicinity after 30 days, except that 4.4 m in shale (overburden) of the UK site. Transport of the dissolved chemicals, via diffusion, is limited to 2.0 m without considering adsorption and less than 0.5 m when the adsorption is considered after 10 years. Moreover, the effect of hydrology condition, strata adsorption properties, and the thermally-induced change of rock porosity and permeability on the propagation of UCG products are studied. The results suggest that unacceptable risks to the

environment are unlikely to arise if standard operating conditions are applied, offering a great prospect of deep coal seams to be considered for UCG. This study also provides insights into the environmental evaluation for other potential UCG projects.

Keywords: Geoenvironment, Numerical methods, Pollution

1. Introduction

As a promising technology, underground coal gasification (UCG) aims to access and harvest the energy contained within the solid fuel underground by converting a coal seam in-situ into synthesis gas, without applying conventional mining methods (Attwood et al., 2003; Bhutto et al., 2013; Sarhosis et al., 2015; Perkins, 2018). This technology has a great potential to contribute to the development of clean coal technologies, when accompanied by the technology of (enhanced) coal bed methane ((E)CBM) and carbon capture and storage (CCS) (Bhutto et al., 2013; Younger, 2011). However, some environmental concerns of UCG technology, e.g. gas emission, groundwater contamination, ground subsidence, were raised by researchers based on site observations (Campbell et al., 1978; Dalton and Campbell, 1978; Humenkk and Maitox, 1977; Imran et al., 2014; Kapusta et al., 2013; Liu et al., 2007; Man et al., 2014; Stuermer et al., 1982). Hence, it is of great importance to enhance the understanding of the potential environmental impact of UCG technology and to develop an environmental assessment of the field-scale UCG trials.

Many efforts have been undertaken towards understanding and evaluating the potential environmental impact of UCG by field investigations (Campbell et al., 1978; Chappell and Mostade, 1998; Humenkk and Maitox, 1977; Kapusta et al., 2013), laboratory experimental work (Dalton and Campbell, 1978; Strugała-Wilczek and Stańczyk, 2016; Wiatowski et al., 2016), and numerical modelling (Otto and Kempka, 2015, 2017; Soukup et al., 2015; Yang and Zhang, 2009). During the UCG reactor operating process, land subsidence was observed, but mainly in the UCG

projects operated at shallow depths and in moderate to thick coal seams (Burton et al., 2017; Creedy et al., 2001; Derbin et al., 2015). However, this can be managed via appropriate site selection based on the depth and thickness of the target coal seam, subsidence estimation and process operation (Kapusta et al., 2013). Besides, the escape of product gases (around 5% to 25%) into the air and surrounding strata occurs due to the unbalance between the elevated reactor pressure and the hydrostatic pressure and it can cause reductions in the coal gasification efficiency (Chappell and Mostade, 1998). During the UCG decommissioning stage, the change of groundwater quality was observed in many field investigations, e.g. Hoe creek UCG trials (Campbell et al., 1978; Dalton and Campbell, 1978;), Hanna site (Lindblom and Smith, 1993; Moody, 1990), Bloodwood Creek UCG site (Mallett, 2018), Barbara coal mine (Kapusta et al., 2013), and laboratory experimental work (Strugała-Wilczek and Stańczyk, 2016; Wiatowski et al., 2016). The types and concentrations of the dissolved chemical species are site-specific and vary depending on coal and ash compositions, gasifier temperatures, and natural water quality.

A minimum depth of 600 m has been suggested for UCG trials in order to encourage the gasifier efficiency and methane production, which also has the potential to reduce the negative environmental impact (Bhutto et al., 2013; Gemmell, 2016). However, the study of the environmental impact of UCG in deep coal seams remains scarce due to the challenging and expensive data extraction from a fully instrumented UCG trial (Gadelle et al., 1982). Therefore, an integrated numerical investigation of the environmental impact of UCG targeting deep coal seams is necessary.

Evaluation of deep-buried coal seams (>900 m) for production of syngas with high-value components is the aim of the MEGAPlus project, as with greater burial depths the gasifier efficiency can be increased, and environmental impact minimized. Three hypothetical sites, i.e. in

the UK, Poland and Germany, studied in the MEGAPlus project, are investigated herein for preliminary assessment of the environmental impact of field-scale UCG via numerical modelling. For this purpose, a series of simulation scenarios are conducted to investigate the gaseous and dissolved chemicals' transport during the UCG reactor operating stage and decommissioning stage in three deep target areas in Europe of specific interest within the MEGAPlus project, i.e. South Wales coalfield (UK), Upper Silesian coal Basin (PL) and Ruhr mining district (DE). A coupled hydro-thermal-chemical (HTC) model developed for UCG application is employed. Moreover, the effect of ground hydrology condition, strata adsorption properties, and the thermally-induced change of rock porosity and permeability on the propagation of UCG products in the reactor's close vicinity are investigated.

2. Site information

Three target areas of specific interest at regional-scale, i.e. UK, PL, and DE sites, proposed in MEGAPlus project are investigated herein. Open access data, e.g. data from the British Geological Survey (BGS) for the UK site, and borehole scans in this project are collected and used to identify and integrate coal seams suitable for the assessment of UCG operations (T Kempka, E Chabab and C Otto 2019, personal communication).

In the central to the western part of the South Wales Basin (UK), the Middle Coal Measure Formation (Westphalian B-C) provides suitable coal seams at depths between 800–1500 m. Based on the borehole information acquired from BGS, "Six Feet" coal seam exhibits the most promising depth, thickness, and occurrence for UCG application at the UK site (T Kempka, E Chabab and C Otto 2019, personal communication). The distribution of the lithostratigraphic units in Upper Silesian coal basin (Poland) shows the potential of seam 510 ("Wesola" coal), with depths between

840–1700 m and a maximum thickness of 13.3 m, to be the major target coal seam in subsequent UCG operation assessment of PL site (T Kempka, E Chabab and C Otto 2019, personal communication).The coal seam is surrounded by claystones/siltstones as well as sandstones/mudstones. In Ruhr mining district (Germany), the Westphalian B Formation provides suitable coal seams for UCG operation, which are at depths between 900 m–1500 m, exhibiting seam thicknesses that vary between 1 m and 3 m (T Kempka, E Chabab and C Otto 2019, personal communication). The targeting seams are separated by sandstones and claystones with mean thicknesses of about 25 m and maximum thicknesses of 220 m. The geological information and the approximate location and extent of the target areas of interest are detailed in Figure 1.

Besides, material properties, including the porosity, density, permeability, and soil water retention (van Genuchten model) parameters relevant to the selected study areas are detailed in Table 1 (T Kempka, E Chabab and C Otto 2019, personal communication). The van Genuchten model parameters of shale provided by Ferrari et al., (2014) are employed in this study due to the absence of its measurement at the UK site.

3. Numerical approach

3.1 Numerical method introduction

COMPASS code is a coupled thermo-hydro-chemical-mechanical (THCM) model, developed at Cardiff University's Geoenvironmental Research Centre for the applications in a various range of geo-environmental and geo-energy areas (Thomas, 1985; Thomas and He, 1998; Thomas et al., 2009; Thomas et al., 2010). The coupled hydro-thermal-chemical (THC) framework of the COMPASS code was further developed herein to study the transport of chemicals in gaseous and aqueous phases involved in the UCG process. It involved the inclusion of the constitutive

relationship that describes the temperature or pressure dependent material parameter and key processes. Specifically, the heat capacity and thermal conductivity of various rocks were introduced as temperature-dependent constitutive relationships (Kosowska-Golachowska et al., 2014; Otto and Kempka, 2015; Tang et al., 2015; Zagorščak et al., 2019) (Table 1). Moreover, geochemical reactions were considered via the equilibrium adsorption/desorption module in COMPASS (Hosking et al., 2018).

The governing equations of liquid, heat and multichemical flows are presented as:

$$\frac{\partial(\rho_l \theta_l)}{\partial t} = -\nabla \rho_l V_l \tag{1}$$

$$\frac{\partial[H_c(T - T_r)]}{\partial t} = -\nabla\left[-\lambda_T \nabla T + \left(C_{pl}\rho_l V_l + C_{pg}\rho_g V_g\right)(T - T_r)\right] \tag{2}$$

$$\frac{\partial(c_j^i n S_j)}{\partial t} = \nabla\left[D_j^i \nabla c_j^i\right] - \nabla\left[c_j^i V_j\right] + s_j^i \tag{3}$$

Where, ρ_l and ρ_g represent the water and gas densities (kg/m^3), respectively; θ_l is the water content; H_c and λ_T are the specific heat capacity (J/(m^3·K) and the thermal conductivity (W/(m·K) of the studied porous media, respectively; T and T_0 are the calculated temperature and the reference temperature (K); C_{pl} and C_{pg} are the specific heat capacity of liquid and air (J/(kg·K), respectively; V_l and V_g are the aqueous and gaseous velocities (m/s), which can be estimated based on Darcy's law; i represents the i^{th} chemical species and j defines the phase of chemicals: gasous (j=1) or aqueous (j=2); c_j^i represents the i^{th} chemical concentration in the j^{th} phase (mol/m^3 for j=1 and mg/L for j=2); n is the porosity of the studied material; S_j is the degree of saturation in the j^{th} phase; D_j^i represents the diffusion coefficient (m^2/s) of the i^{th} chemical species in the j^{th} phase; s_j^i represents the sink/source term. Specifically, the first, second, and third terms in the right-hand side of

equation (3) represent the diffusion, advection, and reactive/adsorption considered for multichemical flows. The adsorption part is considered as the sink/source term:

$$s_j^i = \frac{\partial \rho_s V_E}{\partial t} \tag{4}$$

Where, ρ_s is the solid density (kg/m^3); V_E is the standard gas volume/solute mass adsorbed per unit mass of porous media. The detailed information of the model development, verification, and validation for its application in UCG projects has been presented by An et al. (2020). The model was compared against analytical solutions in the verification process and applied against a former UCG trial (Hoe Creek UCG programme) for validation purpose.

Application of the UCG technology at the three sites is assumed to be conducted following the best practice guidelines, which is keeping the reactor pressure below hydrostatic (Burton et al., 2017). The scale effect of rock mass discontinuities or heterogeneity on its permeability is not considered in this work, allowing the same initial permeability of each strata layer in all directions. Instead of considering the mechanically-induced strata changes along with cavity creation, i.e. the formation of fractures etc., the alteration of the overburden properties, i.e. porosity and permeability, is considered based on the relationships provided in the literature in this preliminary assessment of the effect of TM changes on the transport of chemical species (Akbarzadeh and Chalaturnyk, 2014). It is also assumed that the disturbed zone by the UCG process does not extend sufficiently far that it provides a direct permeable connection between the reactor zone and any overlying aquifers. Experimental investigations on the change of coal porosity up to 873.15 K (Zhao et al., 2010), on that of shale up to 1475.09 K (Liu et al., 2016), and on that of claystone up to 1273.15 K (Tian et al., 2014) have been reported, suggesting that rock porosity is proportional to temperature. The relationships between the variations of rock porosity and temperature for the studied materials (coal,

shale, and claystone) in three sites are detailed in Table 2. The changes of rock permeabilities are considered by (David et al., 1994):

$$\frac{K}{K_0} = \left(\frac{n}{n_0}\right)^{\alpha} \quad (5)$$

Where, n and n_0 are porosity values corresponding to the permeabilities K and K_0, respectively; α is the porosity sensitivity exponent (Table 2).

Considering the mechanism of molecular adsorption represented by different models, the Freundlich isotherm model was employed by Strugała-Wilczek et al. (2021) to describe the adsorption process of the studied chemical species based on the experimental results and data fitting analysis:

$$V_E = K_f c_e^m \quad (6)$$

Where, K_f represents the Freundlich distribution coefficient; c_e is the equilibrium concentration of chemicals; m is the Freundlich exponent, representing the reaction difficulty. More information can be found in Zagorščak et al. (2019) and An et al. (2020).

3.2 Model dimensions and scenarios

The built domain characteristics and the spatial discretization of the three studied domains are detailed in Figure 1. The bottom of the studied zones is placed to represent a depth of 900 m. The model dimensions are 50 m in the X direction and 63 m, 70 m, and 63 m in the Y directions for the UK, PL, and DE sites, respectively. Each domain is discretised with structured quadrilateral meshes with a minimum size of 0.2 m x 0.2 m, which allows sufficient grid refinement in the UCG reactor

vicinity to maintain the numerical accuracy in the studied scenarios, resulting in total element numbers of 3138, 3010, 3138 for the UK, PL, and DE sites, respectively.

During the UCG reactor operating stage (stage 1), the studied syngas components include carbon dioxide (CO_2), nitrogen (N_2), hydrogen(H_2), methane(CH_4), carbon monoxide (CO), ethane (C_2H_6), and hydrogen sulfide (H_2S) (Kapusta et al., 2020) with different gas diffusion coefficients of 1.15×10^{-5}, 2.11×10^{-5}, 1.48×10^{-4}, 2.33×10^{-5}, 2.1×10^{-5}, 1.04×10^{-5} and 1.28×10^{-5} m^2/s at 303.15 K. The gas boundary conditions at the cavity are described by the total gas concentration of 804.4 mol/m^3 with different measured gas molar ratios for UK and PL sites (Kapusta et al., 2020) (Table 3). The initial pore water pressure is considered as depth-dependent. It is assumed that the pore water pressure at the far-field boundary is kept as constant at a value equal to the initial conditions, allowing water flow outwards freely. Other details on the initial and boundary conditions applied in stage 1 are listed in Table 4. Specifically, the temperature at the boundary is assumed to increase linearly from 303.15 to 1273.15 K within the initial 1.3 days and then kept constant at 1273.15 K until the end of the studied period (e.g. Liu et al., 2019). Consequently, the highest total gas pressure at the cavity boundary approaches 8.51 MPa. The aim of this study is to assess the transport of gaseous and dissolved chemicals when best practice guidelines are followed, i.e. when the reactor pressure is below the hydrostatic one. Hence, reactor over-pressurisation is not considered in this preliminary assessment of the environmental impact of field-scale UCG.

The surrounding strata at the PL and DE sites are considered to be initially saturated. Considering the high air entry value of shale, the gas propagation in the surrounding strata is still very limited even when the initial saturation state of the surrounding strata is partially saturated (An et al., 2020). Hence, the initial unsaturation state of UK overburden layer (degree of saturation as 0.98) is assumed for the study purpose of evaluating the potential gas migration in the studied domain. Considering the critical temperature (647.09 K) of water and the temperature limitation (<643.15

K) in the estimation of water viscosity, the degree of saturation in the studied zone is assumed to be equal to its residual capacity when the temperature is higher than 643.15 K, representing a dry porous medium with no mobile liquid water. The studied period is assumed to be 30 days.

Ammonium (NH_4^+), benzene, phenol, chloride (Cl^-), and sulphate (SO_4^{2-}) are observed in UCG wastewater and the filtrates obtained from leaching tests in MEGAPlus project. Hence, they are considered as the typical dissolved species during the UCG decommissioning stage (stage 2). The diffusion coefficients of the five typical dissolved chemicals are 1.95×10^{-9}, 7.54×10^{-10}, 9.79×10^{-10}, 1.54×10^{-9}, and 1.89×10^{-9} m^2/s, respectively, and their concentrations were further experimentally determined (O Šolcová and K Soukup 2019, personal communication; K Kapusta and W Basa 2019, personal communication). The details of initial and boundary conditions applied for the study of solute propagation are presented in Table 5. The studied period is assumed to be 10 years.

Pure diffusion of solute transport is studied in case 1. Robins et al., (2008) observed that in the South Wales coalfield, the piezometric surface is relatively flat compared with the topography and is largely controlled by the elevation of valley bottoms. In case 2, a hydraulic pressure difference of 10 kPa for the studied domain (10 kPa/50m=0.2 kPa/m) is taken as the worst-case scenario (but still plausible) to account for any sub-surface activities, including those associated with the UCG process, that have the potential to modify groundwater head gradients. This value allows the comparison between different sites, considering the domain dimensions and simulation duration. Moreover, the adsorption process of benzene and phenol on raw “Six Feet” coal in UK site and “Wesola” coal in PL site are experimentally determined and expressed by Freundlich isotherm model by Strugała-Wilczek et al., (2021). Hence, both chemicals are selected as the model compounds for the sorption analysis (case 3). Especially, the adsorption parameters of benzene and phenol in the DE site are assumed to be the same as that of PL site due to the similar characteristics

of the studied coal seams in these two sites. Freundlich isotherms describing the adsorption process of benzene and phenol by shale (Bartelt-Hunt et al., 2005; Jabłońska, 2012), and phenol by claystone (Jabłońska, 2012) (Table 1) are also employed herein. The adsorption of benzene by the claystone is not considered due to data deficiency. Moreover, the thermally-induced change of rock porosity and permeability at the completion of stage 1 is considered in case 4 (pure diffusion) and case 5 (diffusion and advection, similar to case 2). Five scenarios considered in stage 2 are listed in Table 6.

4. Results and discussions

4.1 South Wales coalfield (UK site)

The heat propagation and degree of saturation in the coal cavity surrounding strata after 30 days are plotted in Figures 2a and 2b, respectively. The high-temperature region, i.e. higher than 500K, is limited up to 2 m. A small difference between the temperature profiles in different materials is mainly governed by their variations in thermal conductivities and heat capacities which are introduced as temperature-dependent in the model (Zagorščak et al., 2019). The dry fronts move to around 1.7, 1.8 m, and 4.4 m in shale (underburden), coal, and shale (overburden), respectively.

The results of gas propagation are represented by the ratio of the gas concentration at different distances to the fixed gas concentration at the cavity boundary (C/C_{BC}). All gases propagate to around 1.7 m in shale (underburden, Figure 3a) and 1.8 m in coal (Figure 3b), which corresponds to the dry zone generated by the heat propagation after 30 days. Due to the high air entry values and low permeabilities of shale and coal, it is difficult for syngas to transport in these two layers. However, gas propagates to different distances in the overburden shale: carbon dioxide (CO_2) > carbon monoxide (CO) > methane (CH_4) > hydrogen (H_2) > ethane (C_2H_6) > nitrogen (N_2) > hydrogen sulfide (H_2S), which is mainly attributed to the gas transport governed by both diffusion

and advection. Due to its highest gas concentration at the reactor boundary, carbon dioxide (CO_2) moves faster than other gases, approaching around 4.4 m in shale (overburden) with the initially unsaturated condition (Figure 2c and 3c). Figure 2d indicates that porosity increases to different extents in strata surrounding the UCG cavity due to the thermally-induced spalling in a 30-day gasification period. As detailed in Figure 3d, the porosity of coal decreases from 0.65 at the cavity boundary to 0.066 (original value) at around 1.8 m and the porosity of shale goes down gradually from 0.12 at the cavity boundary to 0.05 (original value) at around 1.8 m after 30 days. The thermally-induced porosity change of the strata surrounding the UCG cavity can affect solute propagation, which is further analysed in the UCG decommissioning stage. Overall, with the parameters considered, the risk of the potential gas loss during UCG reactor operating process under normal operating conditions, is estimated to be low at the UK site.

During UCG decommissioning stage, when pure diffusion is considered, sulphate (SO_4^{2-}) moves to around 1.8 m after 10 years in case 1 (Figure 4a). The propagation of ammonium (NH_4^+), benzene, phenol, and chloride (Cl^-) described by the ratio of the solute concentration at different distances to the fixed solute concentration at the cavity boundary (C/C_{BC}) are all limited to around 2.0 m, similar to that of sulphate (SO_4^{2-}) due to their low diffusion coefficient values (Figure 5a). Because of the similar variation tendency of different dissolved chemicals, sulphate (SO_4^{2-}) is selected as a representative species due to its highest concentration among the studied dissolved chemicals. The propagation of sulphate (SO_4^{2-}) in case 2, case 4 and case 5 are presented in Figures 4b, 4e and 4f, respectively. Case 3 is designed to study the propagation of benzene and phenol with considering their adsorption. Hence, the propagation of sulphate (SO_4^{2-}) in case 3, which is the same as that of case 1, is not presented. The results show that sulphate (SO_4^{2-}) moves to around 2.2 m after 10 years in case 2 (diffusion + advection, Figure 4b), slightly further than that of case 1.

The hydraulic gradient allows the dissolved chemicals to move to a slightly further distance, but still limited to the near-cavity zone, which is mainly attributed to the low permeability of coal at the UK site. In Figures 4c and 4d, the propagations of benzene and phenol in case 3 considering adsorption are significantly retarded in the coal and underburden shale layers. Figures 4e and 4f indicate that sulphate (SO_4^{2-}) propagates to around 2.6 m in case 4 and 3.0 m in case 5, respectively, indicating that materials with elevated porosity/permeability allow solutes to transport more quickly. Besides, the detailed propagation of sulphate (SO_4^{2-}) in the coal layer of cases 1, 2, 3, 4, and 5 are plotted in Figure 5b. The comparison between the results of cases 1 and 4, cases 2 and 5 further indicates that the effect of elevated porosity is more significant when diffusion is predominant in solute transport. Figures 5c and 5d present the details of benzene and phenol propagation in the coal layer of cases 1, 2, 3, 4 and 5 after 10 years in the UCG decommissioning phase (stage 2) at the UK site. In case 3 where adsorption is considered, their propagations are limited to the near-cavity zone (less than 0.5 m). The comparisons between the results of benzene and phenol in other cases are similar to that of sulphate (SO_4^{2-}).

4.2 Upper Silesian coal basin (PL site)

During the UCG reactor operating process, the high-temperature regions (Figure 6a), i.e. higher than 500 K, the dry front (Figure 6b), and the propagation of carbon dioxide (CO_2) (Figure 6c), are all limited up to 2 m in the surrounding strata of the PL site. Figures 7a, 7b, and 7c indicate that the propagation distances of different gases in claystone (underburden), coal, and claystone (overburden) are similar, less than 2.0 m. The gas movement is limited to the dry zone in each strata layer generated by the heat propagation. Due to the thermally-induced spalling during the coal gasification process, rock porosity increases to different extents (Figure 6d) in strata

surrounding the UCG cavity. Figure 7d indicates that the porosity of coal decreases from 0.65 at the cavity boundary to 0.06 (original value) at around 1.8 m, and the porosity of claystone goes down gradually from 0.39 at the cavity boundary to 0.06 (original value) at around 1.7 m after 30 days. Due to the high air entry values of coal/claystone and their low permeabilities, it is difficult for the syngas to transport in these materials surrounding the PL UCG reactor. Thereby, there is a low probability of gas loss under normal operating conditions at the PL site.

At the PL site, sulphate (SO_4^{2-}) is selected as a representative species due to its highest value among the studied dissolved chemicals. Sulphate (SO_4^{2-}) moves to around 1.8 m and 2.2 m after 10 years in case 1 (Figure 8a) and case 2 (Figure 8b), respectively. Hence, the hydraulic gradient favours the movement of the dissolved chemicals marginally, which is related to the low permeability of coal at the PL site. Figure 8c shows that benzene in the coal layer has been adsorbed significantly after 10 years. The adsorption of benzene by the bottom claystone is not considered due to the lack of experimental data. Hence, the propagation of benzene is visible in the lower part of the near cavity area, i.e. the claystone layer. In Figure 8d, the propagations of phenol in both coal and underburden claystone layers are significantly retarded due to their adsorption by coal and claystone. Besides, the coal layer with elevated porosity allows sulphate (SO_4^{2-}) propagate to around 2.6 m in case 4 (Figures 8e) and 3.0 m in case 5 (Figures 8f), respectively. The propagation of ammonium (NH_4^+), benzene, phenol, and chloride (Cl^-) are all limited to around 2.0 m, similar to that of sulphate (SO_4^{2-}) due to their similar diffusion coefficient values (Figure 9a). The propagations of sulphate (SO_4^{2-}) (Figure 9b), benzene (Figure 9c) and phenol (Figure 9d) are similar to that of the UK site.

4.3 Ruhr mining district (DE site)

Figures 10a, 10b, and 10c present that the heat propagation, degree of saturation and carbon dioxide (CO_2) propagation in the strata surrounding UCG cavity in the DE site are all limited up to 2 m. Moreover, the propagation distances of different gases in each zone are also similar, less than 2 m (Figure 11a), due to the effect of thermally-induced dry zones. The similar results in PL and DE sites are mainly attributed to their similar strata properties, e.g. rock types, permeabilities and soil water retention characteristics. Thereby, a low risk of the potential gas loss can also be estimated during the UCG reactor operating process of the DE site. Figure 10d shows the elevated rock porosities in the UCG reactor vicinity due to the thermally-induced spalling during a 30-day gasification process. Figure 11d indicates that the porosity of coal drops from 0.61 at the cavity boundary to 0.02 (original value) at around 1.8 m, the porosity of claystone goes down gradually from 0.34 at the cavity boundary to 0.02 (original value) at around 1.7 m and the porosity of sandstone decreases from 0.17 at the cavity boundary to 0.02 (original value) at around 3.7 m after 30 days.

The simulation results of sulphate (SO_4^{2-}) propagation in cases 1, 3, and 4 of the DE site (Figure 12), and the propagation of ammonium (NH_4^+), benzene, phenol, chloride (Cl^-), and sulphate (SO_4^{2-}) in case 1 (Figure 13a) are similar as observed at the UK/PL site. In case 2, when the same hydraulic gradient as that at the UK/PL site is applied in the DE site, sulphate (SO_4^{2-}) moves to around 45 m after nearly 10 years, much further than that of UK/PL sites. It is mainly attributed to the higher coal permeability (1×10^{-14} m^2) at the DE site, which is around two orders of magnitude larger than that of UK/PL sites. Hence, groundwater flow governs the solute transport when both diffusion and advection are considered in case 2. However, adsorption is not considered herein when the advective flow is dominant, hence any results considering groundwater flow represent the worst-

case scenario. Figure 12c indicates that benzene has been adsorbed significantly in the coal layer. The propagations of phenol in both coal and underburden claystone layers are retarded due to the adsorption process (Figure 12d). Figures 12e and 13b indicate that coal with elevated porosity can favour the propagation of sulphate (SO_4^{2-}) when pure diffusion is considered (case 4). However, comparing to the results of case 2, the propagation of sulphate (SO_4^{2-}) is retarded significantly in case 5. Due to the increased permeability in the porosity influenced zone, the hydraulic pressure is redistributed in the reactor vicinity (from the reactor boundary to the distance of 1.8 m), as shown in Figure 13b. Hence in this zone, the movement of sulphate (SO_4^{2-}) is governed by diffusion, leading to the concentration of sulphate (SO_4^{2-}) varying from 2250.0 mg/L at the cavity boundary to 1983.4 mg/L at around 1.8 m after 10 years. Beyond that, the existing hydraulic gradient enhances the propagation of sulphate (SO_4^{2-}), allowing sulphate (SO_4^{2-}) move to around 37 m after 10 years. Moreover, Figures 13c and 13d indicate that the propagation of benzene and phenol is similar to that of sulphate (SO_4^{2-}) when adsorption is not considered. It needs to be noted that, an increase in permeability with the same hydraulic gradient can increase the flow velocities together with the associated transport of contaminants by advection. However, at the DE site, the retardation of the solutes' transport in case 5 compared to that of case 2 is obtained by the numerical investigation based on the assumption of a fixed hydraulic gradient in the studied domain and the changed porosity and permeability of the coal seam. More investigation is still required to clarify the existing hydrology condition and the change in porosity and permeability of the studied materials at the UCG site. When adsorption is considered in case 3, the propagation of benzene and phenol is limited to the near-cavity zone (less than 0.5 m).

4.4 Discussions

Syngas loss is the predominant potential environmental risk during the UCG reactor operating stage (stage 1), which carries the gaseous contaminants to a further distance away from the reactor and which then can condense at the low-temperature zone (Bhutto et al., 2013; Burton et al., 2017). The numerical investigations of the potential gaseous propagation at three sites demonstrate that the initial saturation of strata surrounding the UCG reactor, the properties of the materials (e.g. water retention curves, porosity, and permeability), and the produced gas component (e.g. gas diffusion coefficients and concentrations) are the main drivers for different gas behaviours. Especially, the strata layers with high air entry values and low permeabilities can minimize gas propagation. The assumed initially unsaturated state of the strata layer can favour the gases propagate to a further distance, e.g. the overburden shale layer of UK site. Thereby, assessment of the initial saturation of strata, which might be impacted by previous activities (e.g. CBM or dewatering to initiate the UCG process), or natural occurrences (e.g. confined/unconfined aquifers) is important in the estimation of gas propagation. A better understanding of the potential syngas migration in coal can also help in identifying the proper width of the safety pillars between the UCG reactors, avoiding the potential gas escape from one cavity to another, and underestimation of gas loss from the reactor.

During the UCG decommissioning stage (stage 2), transport of the studied dissolved chemicals via diffusion are all limited to 1.0~2.0 m after 10 years in the surrounding strata of UK, PL, and DE sites (Figures 5a, 9a, and 13a). The hydraulic gradient can enhance the propagation of the dissolved chemicals to different extents, which are determined by the permeability of the rock layer along with the hydraulic gradient. Thereby, the initial assessment of hydrogeology condition and the regular check-ups of its condition in the area of the interest is required to evaluate the propagation

of dissolved chemicals in UCG surrounding strata for the short-term. Moreover, as the groundwater drawdown changes are expected to recover to near pre-operational levels few years after the UCG termination (Campbell et al., 1978; Camp and White, 2015), ensuring that a sufficient distance between the UCG reactor and any potential conduits (e.g. faults or other high permeability strata) is essential to prevent any migration of chemicals outside the UCG reactor zone.

When adsorption of different chemicals (phenol and benzene) is considered, it is shown that their propagations are limited to the near-cavity zone (less than 0.5 m). Hence, deep coal seams (>900 m) and their surrounding strata as identified in the three sites of interest present a good prospect to be utilized for the UCG purpose. Hence, understanding the adsorption characteristics of various UCG-relevant dissolved chemicals on different rock materials surrounding the UCG reactor is essential for reliable assessment of such phenomena, bringing the benefits of the surrounding rock as a potential natural buffer. However, alternative scenarios that consider different pathways between the contaminant source (UCG cavity) and receptors when multiple UCG modules operate need to be further investigated.

The process of the UCG reactor operating stage is also accompanied by heating of the surrounding strata, including cavity overburden, floor rocks of the coal bed, and subsurface waters. It is well known that an increase of rock temperature leads to a change in rock porosity and permeability (David et al., 1994; Zhao et al., 2010; Tian et al., 2014; Liu et al., 2016). Based on the investigation results of three sites (cases 4 and 5), the enhanced transport properties, i.e., thermally-induced porosity/permeability change, of the surrounding strata enhance the solute propagation in the surrounding strata when diffusion is predominant. However, the thermally-induced spalling may also retard the solute propagation when the groundwater flow predominantly affects the solute transport, as seen at the DE site when the fixed hydraulic gradient was applied at the studied domain.

5. Conclusions

Based on the numerical investigation of gaseous and dissolved chemicals' propagation at the UK, PL and DE sites, the following conclusions can be drawn:

- At the end of the gasification stages at the three studied sites, the gas propagation is limited to the proximity of the UCG reactor and is correlated to the high-temperature zone formed around it, i.e. 1.0~2.0 m in the surrounding strata after 30 days. The assumed initially unsaturated state of the overlaying shale layer in the UK site favours the gas propagation to a slightly further distance (4.4 m) in the reactor overburden compared to other sites. Thereby, except the soil water retention characteristics and permeabilities of the field materials, the initial saturation in strata surrounding the UCG reactor is also essential for the accurate evaluation of the gas propagation during UCG reactor operating process.
- The transport of non-adsorbing dissolved chemicals via diffusion is limited to the near-cavity area after 10 years (up to 2.0 m) in all studied areas owing to the low porosity of the strata surrounding the UCG reactors. When adsorption is considered, the propagation of the studied chemicals via diffusion is limited to the near-cavity zone (less than 0.5 m), suggesting a good prospect of deep geological strata as a buffer which serves to retard the movement of chemical species. This highlights the importance of site-specific assessment of adsorption characteristics of different rock materials surrounding the UCG reactors, which is essential for reliable assessment of UCG's environmental impact and can show the benefits of the surrounding rock as a potential natural buffer in the long term.
- The transport of dissolved chemicals could be affected by the potential groundwater flow and alteration of strata surrounding the UCG reactor, as demonstrated for all three sites. Although groundwater flow at such depths is expected to be limited, any sub-surface activities, including

those associated with the UCG, have the potential to modify groundwater head gradients and hence, this needs to be properly assessed. However, adsorption is not considered herein when the advective flow is dominant, hence any results considering groundwater flow represent the worst-case scenario. The thermally-induced porosity/permeability change in strata layers favours the solute propagation when diffusion is predominant. However, the thermally-induced spalling may also retard the solute propagation when the groundwater flow predominantly affects the solute transport, as seen at the DE site. Possible thermo-mechanical changes in overlaying strata due to long/multiple UCG panels and potential failure of well-seals may also lead to changes in their permeabilities, soil water retention properties, and saturation state, which will be considered in future research on UCG large scale modelling by the authors.

- Overall, the simulation results suggest that, following the best practice guidelines, i.e. to keep reactor pressure below the hydrostatic and reduce the disturbance to the near-reactor area without a direct permeable connection between the reactor zone and any overlying aquifers, deep geological formations (below 900 m) at the UK, PL and DE sites of interest offer a good prospect for UCG utilization. Attention needs to be paid to the potential impact of groundwater flow and thermo-mechanical changes above the reactor(s), which need to be identified and assessed during the site selection process. This study also provides insights into the potential environmental evaluation for other similar UCG projects.

Acknowledgements

This work was supported by the EU Research Fund for Coal and Steel (RFCS) as a part of the MEGAPlus project (Grant Agreement number 800774-MEGAPlus-RFCS-2017). The financial support is gratefully acknowledged.

Reference

Akbarzadeh H and Chalaturnyk RJ (2014) Structural changes in coal at elevated temperature pertinent to underground coal gasification: A review. International Journal of Coal Geology **131**: 126–146. doi: https://doi.org/10.1016/j.coal.2014.06.009.

Alderton DHM, Oxtoby N, Brice H et al. (2004) The link between fluids and rank variation in the South Wales Coalfield: evidence from fluid inclusions and stable isotopes. Geofluids **4(3)**: 221–236. doi: https://doi.org/10.1111/j.1468-8123.2004.00083.x

An N, Zagorščak R, Thomas HR and Gao W (2020) A numerical investigation into the environmental impact of underground coal gasification technology based on a coupled thermal-hydro-chemical model. Journal of Cleaner Production **125181**, ISSN 0959-6526. https://doi.org/10.1016/j.jclepro.2020.125181.

Attwood T, Fung V and Clark WW (2003) Market opportunities for coal gasification in China. Journal of Cleaner Production **11(4)**: 473–479. doi: https://doi.org/10.1016/S0959-6526(02)00068-9.

Bartelt-Hunt SL, Smith JA, Burns SE et al. (2005) Evaluation of granular activated carbon, shale, and two organoclays for use as sorptive amendments in clay landfill liners. Journal of Geotechnical and Geoenvironmental Engineering **131(7)**: 848–856, https://doi.org/10.1061/(ASCE)1090-0241(2005)131.

Bevins RE, White SC and Robinson D (1996) The South Wales coalfield: low grade metamorphism in a foreland basin setting? Geological Magazine **133(6)**: 739–49. https://doi.org/10.1017/S0016756800024584

Bhutto AW, Bazmi AA and Zahedi G (2013) Underground coal gasification: From fundamentals to applications. Progress in Energy and Combustion Science **39(1)**: 189–214. doi: https://doi.org/10.1016/j.pecs.2012.09.004.

Bukowska M and Smolorz A (2019) Influence of Humidity on the Energy of Specific Strain in the Process of Loading Sedimentary Rocks. Studia Geotechnica et Mechanica **41(4)**: 223-230. doi: https://doi.org/10.2478/sgem-2019-0033

Burton E, Friedmann J and Upadhye R (2017) Best Practices in Underground Coal Gasification. No. LLNL-TR-225331. Lawrence Livermore National Lab, Livermore, CA, United States.

Camp DW and White JA (2015) Underground Coal Gasification: An Overview of Groundwater Contamination Hazards and Mitigation Strategies. No. LLNL-TR-668633. Lawrence Livermore National Lab, Livermore, CA, United States.

Campbell JH, Pellizzari E and Santor S (1978) Results of a Groundwaer Quality Study near an Underground Coal Gasification Experiment (Hoe Creek I). Rept. UCRL-52405. Lawrence Livermore National Lab, Livermore, CA, United States.

Chappell R and Mostade M (1998) The EL Tremedal underground coal gasification field test in Spain first trial at great depth and high pressure. In *the Fifteenth Annual International Pittsburgh Coal Conference*. Pittsburgh, USA, pp. 1–19.

Creedy DP, Garner K, Holloway S et al. (2001) Review of Underground Coal Gasification Technological Advancements. Contract No.: COAL R211/Pub URN 01/1041. Harwell Laboratory, Coal R & D Programme.

Dalton VA and Campbell JH (1978) Laboratory measurement of groundwater leaching and transport of polluants produced during underground coal gasification. IN SITU **2(4)**: 295–328.

David C, Wong TF, Zhu W et al. (1994) Laboratory measurement of compaction-induced permeability change in porous rocks: Implications for the generation and maintenance of pore pressure excess in the crust. Pure and Applied Geophysics **143(1–3)**: 425–456. doi: https://doi.org/10.1007/BF00874337.

Derbin Y, Walker J, Wanatowski D et al. (2015) Soviet experience of underground coal gasification focusing on surface subsidence. Journal of Zhejiang University: Science A **16(10)**: 839–850. doi: https://doi.org/10.1631/jzus.A1500013.

Ekneligoda TC and Marshall AM (2018) A coupled thermal-mechanical numerical model of underground coal gasification (UCG) including spontaneous coal combustion and its effects. International Journal of Coal Geology **199(May)**: 31–38. doi:https://doi.org/10.1016/j.coal.2018.09.015.

Ferrari A, Favero V, Marschall P et al. (2014) Experimental analysis of the water retention behaviour of shales. International Journal of Rock Mechanics and Mining Sciences **72**: 61–70. doi: https://doi.org/10.1016/j.ijrmms.2014.08.011.

Gadelle C, Lessi J and Sarda JP (1982) Underground Coal Gasification at Great Depth. The French Field Test of Bruay-En-Artois. Revue de L Institut Francais du Petrole **37(2)**: 157–181.

Gemmell C (2016) Independent Review of Underground Coal Gasification – Report. A Report to the Scottish Government, Edinburgh, UK.

Hosking LJ, Thomas HR and Sedighi M (2018) A dual porosity model of high-pressure gas flow for geoenergy applications. Canadian Geotechnical Journal **55(6)**: 839–851. doi: https://doi.org/10.1139/cgj-2016-0532.

Humenkk MJ and Maitox CF (1977) Groundwater Pollutants From Underground Coal Gasification. Water Research **12(7)**: 463–469, https://doi.org/10.1016/0043-1354(78)90153-7.

Imran M, Kumar D, Kumar N et al. (2014) Environmental concerns of underground coal gasification. Renewable and Sustainable Energy Reviews **31**: 600–610. doi: https://doi.org/10.1016/j.rser.2013.12.024.

Jabłońska B (2012) Sorption of phenol on rock components occurring in mine drainage water sediments. International Journal of Mineral Processing **104–105**: 71–79. doi: https://doi.org/10.1016/j.minpro.2011.12.008.

Kapusta K, Stańczyk K, Wiatowski M et al. (2013) Environmental aspects of a field-scale underground coal gasification trial in a shallow coal seam at the Experimental Mine Barbara in Poland. Fuel **113**: 196–208. doi: https://doi.org/10.1016/j.fuel.2013.05.015.

Kapusta K, Wiatowski M, Stanczyk K et al. (2020) Large-scale Experimental Investigations to Evaluate through Underground Coal Gasification Process. Energies **13(6)**: 1334.

Kędzior S (2015) Methane contents and coal-rank variability in the Upper Silesian Coal Basin, Poland. International Journal of Coal Geology **139**: 152–164. doi: https://doi.org/10.1016/j.coal.2014.09.009

Kosowska-Golachowska M, Gajewski W and Musiał T (2014) Determination of the effective thermal conductivity of solid fuels by the laser flash method. Archives of Thermodynamics **35(3)**: 3–16. doi: https://doi.org/10.2478/aoter-2014-0018.

Lindblom S and Smith V (1993) Rocky Mountain 1 Under Ground Coal Gasification Test, Hanna Wyoming Ground Water Evaluation. Laramie, Wyoming.

Liu SQ, Li JG, Mei M et al. (2007) Groundwater Pollution from Underground Coal Gasification. Journal of China University of Mining and Technology **17(4)**: 467–472. doi: https://doi.org/10.1016/S1006-1266(07)60127-8.

Liu X, Guo G and Li H (2019) Study on the propagation law of temperature field in surrounding rock of underground coal gasification (UCG) combustion cavity based on dynamic thermal parameters. Results in Physics **12(4)**: 1956–1963. doi: https://doi.org/10.1016/j.rinp.2019.02.006.

Liu X, Yuan S, Sieffert Y et al. (2016) Changes in Mineralogy, Microstructure, Compressive Strength and Intrinsic Permeability of Two Sedimentary Rocks Subjected to High-Temperature Heating. Rock Mechanics and Rock Engineering **49(8)**: 2985–2998. doi: https://doi.org/10.1007/s00603-016-0950-z.

Mallett CW (2018) Environmental controls for underground coal gasification. Proceedings of the Institution of Mechanical Engineers, Part A: Journal of Power and Energy **232(1)**: 47–55. doi: https://doi.org/10.1177/0957650917723733.

Man Y, Yang S, Xiang D et al. (2014) Environmental impact and techno-economic analysis of the coal gasification process with/without CO2 capture. Journal of Cleaner Production **71**: 59–66. doi: https://doi.org/10.1016/j.jclepro.2013.12.086.

Mao F (2016) Underground coal gasification (UCG): A new trend of supply-side economics of fossil fuels. Natural Gas Industry B **3(4)**: 312–322. doi: https://doi.org/10.1016/j.ngib.2016.12.007.

Moody CG (1990) Changes in groundwater quality and subsurface hydrology during the rocky mountain 1 underground coal gasification test, Hanna, Wyoming.

Nakaten N, Schlüter R, Azzam R et al. (2014) Development of a techno-economic model for dynamic calculation of cost of electricity, energy demand and CO2 emissions of an integrated UCG-CCS process. Energy **66**: 779–790. doi: https://doi.org/10.1016/j.energy.2014.01.014.

Neville George T (1970) British Regional Geology: South Wales, 3rd edn, HMSO, London, UK.

Otto C and Kempka T (2015) Thermo-mechanical simulations of rock behavior in underground coal gasification show negligible impact of temperature-dependent parameters on permeability changes. Energies **8(6)**: 5800–5827. doi: https://doi.org/10.3390/en8065800.

Otto C and Kempka T (2017) Prediction of steam jacket dynamics and water balances in underground coal gasification. Energies **10(6)**: 739. doi: https://doi.org/10.3390/en10060739.

Perkins G (2018) Underground coal gasification – Part I: Field demonstrations and process performance. Progress in Energy and Combustion Science **67**: 158–187. doi: https://doi.org/10.1016/j.pecs.2018.02.004.

Robins NS, Davies J and Dumpleton S (2008) Groundwater flow in the South Wales coalfield: historical data informing 3D modelling. Quarterly Journal of Engineering Geology and Hydrogeology **41(4)**: 477–486. https://doi.org/10.1144/1470-9236/07-055

Sarhosis V, Lavis S, Mostade M et al. (2015) Towards commercialising underground coal gasification in the EU. Environmental Geotechnics **4(2)**: 113–122. doi: https://doi.org/10.1680/jenge.15.00044.

Soukup K, Hejtmánek V, Čapek P et al. (2015) Modeling of contaminant migration through porous media after underground coal gasification in shallow coal seam. Fuel Processing Technology **140**: 188–197. doi: https://doi.org/10.1016/j.fuproc.2015.08.033.

Strugała-Wilczek A, Basa W, Kapusta K et al. (2021) In situ sorption phenomena can mitigate potential negative environmental effects of underground coal gasification (UCG)-an experimental study of phenol removal on UCG-derived residues in the aspect of contaminant retardation. Ecotoxicology and Environmental Safety **208**: 111710. https://doi.org/10.1016/j.ecoenv.2020.111710

Strugała-Wilczek A and Stańczyk K (2016) Leaching behaviour of metals from post-underground coal gasification cavity residues in water differing in mineralization. Fuel **173**: 106–114. doi: https://doi.org/10.1016/j.fuel.2016.01.046.

Stuermer DH, Ng DJ and Morris CJ (1982) Organic Contaminants in Groundwater near an Underground Coal Gasification Site in Northeastern Wyoming. Environmental Science and Technology **16(9)**: 582–587. doi: https://doi.org/10.1021/es00103a009.

Tang F, Wang L, Lu Y et al. (2015) Thermophysical properties of coal measure strata under high temperature. Environmental Earth Sciences **73(10)**: 6009–6018. doi: https://doi.org/10.1007/s12665-015-4364-0.

Thomas HR (1985) Modelling two-dimensional heat and moisture transfer in unsaturated soils, including gravity effects. International Journal for Numerical and Analytical Methods in Geomechanics **9(6)**: 573 – 588. doi: https://doi.org/10.1002/nag.1610090606.

Thomas HR, Cleall P, Li YC et al. (2009) Modelling of cryogenic processes in permafrost and seasonally frozen soils. Geotechnique **59(3)**: 173–184. doi: https://doi.org/10.1680/geot.2009.59.3.173.

Thomas HR and He Y (1998) Modelling the behaviour of unsaturated soil using an elastoplastic constitutive model. Géotechnique **48(5)**: 589–603. doi: https://doi.org/10.1680/geot.1998.48.5.589.

Thomas HR, Vardon PJ and Li YC (2010) Coupled Thermo-Hydro-Chemo-Mechanical Modeling for Geoenvironmental Phenomena. In *Advances in Environmental Geotechnics*. Springer, Berlin, Heidelberg, Germany, pp. 320–327.

Tian H, Ziegler M and Kempka T (2014) Physical and mechanical behavior of claystone exposed to temperatures up to 1000°C. International Journal of Rock Mechanics and Mining Sciences **70**: 144–153. doi: https://doi.org/10.1016/j.ijrmms.2014.04.014.

Wiatowski M, Kapusta K, Ludwik-Pardała M et al. (2016) Ex-situ experimental simulation of hard coal underground gasification at elevated pressure. Fuel **184**: 401–408. doi: https://doi.org/10.1016/j.fuel.2016.07.020.

Yang L and Zhang X (2009) Modeling of Contaminant transport in Underground Coal Gasification. Energy and Fuels **23**: 193–201. doi: https://doi.org/10.1017/CBO9781107415324.004.

Younger PL (2011) Hydrogeological and Geomechanical Aspects of Underground Coal Gasification and its Direct Coupling to Carbon Capture and Storage. Mine Water and the Environment **30(2)**: 127–140. doi: https://doi.org/10.1007/s10230-011-0145-5.

Zagorščak R, An N, Palange R et al. (2019) Underground coal gasification – A numerical approach to study the formation of syngas and its reactive transport in the surrounding strata. Fuel **253(April)**: 349–360. doi: https://doi.org/10.1016/j.fuel.2019.04.164.

Zhao Y, Qu F, Wan Z et al. (2010) Experimental investigation on correlation between permeability variation and pore structure during coal pyrolysis. Transport in Porous Media **82(2)**: 401–412. doi: https://doi.org/10.1007/s11242-009-9436-8.

Table captions

Table 1. Material properties relevant to the selected study areas.

Table 2. The fitting porosity-temperature relationship and the value of α in the estimation of porosity-permeability relationship for the studied materials.

Table 3. Average gas concentrations in gasification experiments on coals from the UK and PL sites (Kapusta et al., 2020).

Table 4. Initial and boundary conditions used in the simulations to investigate potential syngas migration in the reactor vicinity during the UCG operational phase (stage 1).

Table 5. Initial and boundary conditions used in the simulations to investigate the transport of dissolved chemical species in the reactor vicinity during the UCG decommissioning phase (stage 2).

Table 6. Scenarios considered to investigate solute (contaminant) transport during the UCG decommissioning phase (stage 2).

Figure captions

Figure 1. (a-1) Simplified geological map of the South Wales coal basin (UK site) (after Neville George (1970), Bevins et al. (1996), and Alderton et al. (2004)) and the approximate location and extent of the studied area (5 km×5 km) as indicated by the red rectangle; (a-2) the domains of the target area of interest at the UK site and its spatial discretisation; (b-1) simplified geological map

of the Upper Silesian coal basin (PL site) (after Bukowska and Smolorz (2019) and Kedzior (2015)) and the approximate location and extent of the studied area (10 km×6 km) as indicated by the red rectangle; (b-2) the domains of the target area of interest at the PL site and its spatial discretisation; (c-1) geological overview of the Ruhr mining district (DE site) location (modified from the geological overview of the GeoPark Ruhrgebiet, see https://www.geopark.ruhr/en/geopark/ueber-uns/); and (c-2) the domains of the target area of interest at the DE site and its spatial discretisation.

Figure 2. Results of the simulation in the UCG operational phase (stage1): a) temperature (K); b) degree of saturation (-); c) carbon dioxide (CO_2) concentration (mol/m^3) and d) porosity changes in strata surrounding the UCG cavity created by thermally-induced spalling after a 30 day gasification period at the UK site.

Figure 3. Results of the gas propagation in: a) shale (underburden), b) coal (middle layer), and c) shale (overburden); and d) porosity changes after 30 days in the UCG operational phase (stage1) at the UK site.

Figure 4. Results of the simulation after 10 years in the UCG decommissioning phase (stage 2) of the UK site: a) concentration of sulphate (SO_4^{2-}) (mg/L) under diffusive flow (case 1); b) concentration of sulphate (SO_4^{2-}) (mg/L) considering diffusion and groundwater flow (case 2); c) concentration of benzene (mg/L) considering diffusion and adsorption (case 3); d) concentration of phenol (mg/L) considering diffusion and adsorption (case 3); e) concentration of sulphate (SO_4^{2-}) (mg/L) considering diffusion in strata surrounding the UCG cavity affected by thermally-induced spalling (case 4) and f) concentration of sulphate (SO_4^{2-}) (mg/L) considering diffusion and groundwater flow in strata surrounding the UCG cavity affected by thermally-induced spalling (case 5).

Figure 5. The propagation of a) ammonium (NH_4^+), benzene, phenol, chloride (Cl^-), and sulphate (SO_4^{2-}) in case 1; and b) sulphate (SO_4^{2-}), c) benzene and d) phenol in the coal layer of cases 1, 2, 3, 4 and 5 after 10 years in the UCG decommissioning phase (stage 2) at the UK site.

Figure 6. Results of the simulation in the UCG operational phase (stage1): a) temperature (K); b) degree of saturation (-); c) carbon dioxide (CO_2) concentration (mol/m^3); and d) porosity changes in strata surrounding the UCG cavity created by thermally-induced spalling after a 30 day gasification period at the PL site.

Figure 7. Results of the gas propagation in a) claystone (underburden), b) coal (middle layer), and c) claystone (overburden); and d) porosity changes after 30 days in the UCG operational phase (stage1) at the PL site.

Figure 8. Results of the simulation after 10 years in the UCG decommissioning phase (stage 2) of the PL site: a) concentration of sulphate (SO_4^{2-}) (mg/L) under diffusive flow (case 1); b) concentration of sulphate (SO_4^{2-}) (mg/L) considering diffusion and groundwater flow (case 2); c) concentration of benzene (mg/L) considering diffusion and adsorption (case 3); d) concentration of phenol (mg/L) considering diffusion and adsorption (case 3); e) concentration of sulphate (SO_4^{2-}) (mg/L) considering diffusion in strata surrounding the UCG cavity affected by thermally-induced spalling (case 4); and f) concentration of sulphate (SO_4^{2-}) (mg/L) considering diffusion and groundwater flow in strata surrounding the UCG cavity affected by thermally-induced spalling (case 5).

Figure 9. The propagation of a) ammonium (NH_4^+), benzene, phenol, chloride (Cl^-), and sulphate (SO_4^{2-}) in case 1; and b) sulphate (SO_4^{2-}), c) benzene and d) phenol in the coal layer of cases 1, 2, 4 and 5 after 10 years in the UCG decommissioning phase (stage 2) at the PL site.

Figure 10. Results of the simulation in the UCG operational phase (stage1): a) temperature (K); b) degree of saturation (-); c) carbon dioxide (CO_2) concentration (mol/m^3); and d) porosity changes in strata surrounding the UCG cavity created by thermally-induced spalling after a 30 day gasification period at the DE site.

Figure 11. Results of the gas propagation in a) claystone (underburden), b) coal (middle layer), and c) sandstone (overburden); and d) porosity changes after 30 days during UCG operational phase (stage1) at the DE site.

Figure 12. Results of the simulation after 10 years at the UCG decommissioning phase (stage 2) of the DE site: a) concentration of sulphate (SO_4^{2-}) (mg/L) under diffusive flow (case 1); b) concentration of sulphate (SO_4^{2-}) (mg/L) considering diffusion and groundwater flow (case 2); c) concentration of benzene (mg/L) considering diffusion and adsorption (case 3); d) concentration of phenol (mg/L) considering diffusion and adsorption (case 3); e) concentration of SO_4^{2-} (mg/L) considering diffusion in strata surrounding the UCG cavity affected by thermally-induced spalling (case 4); and f) concentration of sulphate (SO_4^{2-}) (mg/L) considering diffusion and groundwater flow in strata surrounding the UCG cavity affected by thermally-induced spalling (case 5).

Figure 13. The propagation of a) ammonium (NH_4^+), benzene, phenol, chloride (Cl^-), and sulphate (SO_4^{2-}) in case 1; and b) sulphate (SO_4^{2-}), c) benzene and d) phenol in the coal layer of cases 1, 2, 4 and 5 after 10 years in the UCG decommissioning phase (stage 2) at the DE site.